Increased Frame Rate for Plane Wave Imaging Without Loss of Image Quality

Jensen, Jonas; Stuart, Matthias Bo; Jensen, Jørgen Arendt

Published in:
Proceedings of IEEE International Ultrasonics Symposium

Link to article, DOI:
10.1109/ULTSYM.2015.0312

Publication date:
2015

Document Version
Peer reviewed version

Increased Frame Rate for Plane Wave Imaging Without Loss of Image Quality

Jonas Jensen, Matthias Bo Stuart and Jørgen Arendt Jensen

Center for Fast Ultrasound Imaging, Dept. of Elec. Eng. Bldg. 349,
Technical University of Denmark, DK-2800 Lyngby, Denmark

***Abstract*—Clinical applications of plane wave imaging necessitate the creation of high-quality images with the highest possible frame rate for improved blood flow tracking and anatomical imaging. However, linear array transducers create grating lobe artefacts, which degrade the image quality especially in the near field for λ-pitch transducers. Artefacts can only partly be suppressed by increasing the number of emissions, and this paper demonstrates how the frame rate can be increased without loss of image quality by using λ/2-pitch transducers. The number of emissions and steering angles are optimized in a simulation study to get the best images with as high a frame rate as possible. The optimal setup for a simulated 4.1 MHz λ-pitch transducer is 73 emissions and a maximum steering of 22°. The achieved FWHM is 1.3λ and the cystic resolution is -25 dB for a scatter at 9 mm. Only 37 emissions are necessary within the same angle range when using a λ/2-pitch transducer, and the cystic resolution is reduced to -56 dB. Measurements are performed with the experimental SARUS scanner connected to a λ-pitch and λ/2-pitch transducer. A wire phantom and a tissue mimicking phantom containing anechoic cysts are scanned and show the performance using the optimized sequences for the transducers. Measurements confirm results from simulations, and the λ-pitch transducer show artefacts at undesirable strengths of -25 dB for a low number of emissions.**

I. Introduction

Medical ultrasound synthetic aperture imaging (SA) solves the limitations in conventional line-by-line imaging, which has a reduced frame rate and only optimal focusing at one depth. SA has been used with spherical waves [1], [2] and plane waves (PW) [3], [4]. By using emissions with wide areas of insonification, a low-resolution (LR) image is created for each emission, however, each LR image has low contrast. To regain contrast, LR images are combined to high-resolution (HR) images at the cost of a reduced frame rate. For anatomical imaging [5], [6] and flow estimation [7]–[9], it is important to use as few emissions as possible to keep the frame rate high and still obtain high-quality images.

The spatial sampling of a transducer aperture into array elements with λ-pitch results in aliasing of spatial frequencies. An unfocused emission from a transducer with a pitch equal to the pulse wavelength, λ, generates grating lobes in the emitted pressure field as illustrated in Fig. 1. A steered plane wave at 10° is simulated, and a grating lobe behind the wave front has amplitudes around -25 dB, which introduce artefacts in a beamformed image. Grating lobe artefacts can be suppressed by increasing the number of emissions, however, a λ/2-pitch transducer avoids grating lobes and can therefore potentially increase the frame rate without compromising the image quality.

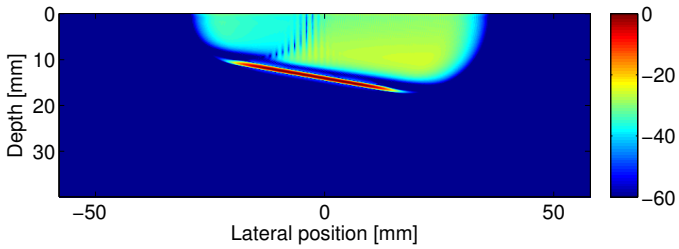

Fig. 1. Field II simulation of emitted field from a λ-pitch transducer, when a plane wave is emitted at 10 deg.

Small parts SA/PW imaging in related work [5]–[9] have so far been conducted with commercially available λ-pitch transducers, which are actually intended for line-by-line imaging with no steering. The pitch size is a compromise between having a high center frequency and a wide aperture to get a large field of view for small parts imaging, and the limitation of 128-192 channels in commercial scanners. Therefore, a transducer with the same aperture size and a pitch around λ/2 can only be obtained by using more channels, a lower center frequency, or not sampling all elements.

This paper investigates the image quality of PW images using a λ/2-pitch transducer and compares it to a conventional λ-pitch transducer. The relationship between image quality and frame rate is investigated for both transducers, and it is shown that a higher frame rate can be obtained by using a λ/2-pitch transducer compared to a λ-pitch transducer without loss of image quality. For a fair comparison between the transducers, a method for selecting the number of PW emissions and maximum steering angle based on the optimal image quality is presented. The method is presented with a simulation study in Section II. In Section III, methods for implementing the approach on the experimental scanner SARUS are described. The results of phantom measurements are presented in Section IV.

II. Optimization Procedure

A procedure for optimizing the image quality in terms of detail resolution and contrast is conducted for a λ-pitch and λ/2-pitch transducer. The detail resolution is quantified as the full width at half maximum (FWHM), while the contrast is

TABLE I
PARAMETERS USED FOR SIMULATION AND MEASUREMENTS.

Parameter	**λ-pitch**	**λ/2-pitch**
Number of elements	96	192
Center frequency f_0	4.1 MHz	4.1 MHz
Cycles in emitted pulse	1	1
Wavelength λ	0.376 mm	0.376 mm
Element pitch	0.4 mm	0.2 mm
Element height	6 mm	6 mm
Elevation focus	38 mm	38 mm
Transmit apodization	Tukey (weight 0.5)	Tukey (weight 0.5)
Receive apodization	Hamming	Hamming
Receive F-number	1	1

accessed through the cystic resolution (CTR), which quantifies the side lobe energy of the point-spread-function (PSF) outside a 4λ radius of the main lobe. The independent variables for the optimization procedure are the maximum steering angle, α_{max}, and the number of PWs, N, while the dependent variables are FWHM and CTR. The procedure is applied on simulated data and uses Pareto efficiency [10]. A Pareto frontier is constructed, which represent solutions, where it is impossible to improve one of the variables (CTR or FWHM) without worsening the other. Thereby, attention can be restricted only to solutions that are Pareto efficient, wherein trade-offs can be made, rather than considering all the solutions.

The actual pitches of the transducers are 1.12λ and 0.56λ, respectively, due to the experimental equipment available for small parts imaging. The λ/2-pitch transducer has twice as many elements as the λ-pitch transducer to obtain the same aperture width. Parameters are listed in Table I. Five point targets are simulated at axial distances of 9, 20, 34, 44, and 60 mm from the transducer surface (corresponding to a scanned wire phantom). Simulations are performed using the Field II program [11], [12]. A Tukey apodization on the active transmit aperture is applied to reduce artefacts from edge waves. Plane wave emissions with steering angles from -40° to +40° and with 0.25° separation between each plane wave are simulated, and beamformation is performed using the BFT3 toolbox [13]. The beamformed low-resolution images are subsequently combined to high-resolution images with all combinations of α_{max} and N.

A scatter plot of lateral FWHM and CTR for all the HR images of a scatter at 9 mm is shown in Fig. 2 for the λ-pitch transducer. Axial FWHM are not included, since they are approximately λ in all cases. Solutions that are Pareto optimal are shown as black and the Pareto frontier as a black curve in Fig. 2. Any of the solutions on the Pareto frontier can be selected and used as a Pareto efficient setup for the given depth.

An interesting solution is at the knee point of the frontier, since it represents a trade-off between FWHM and CTR. However, since a Pareto frontier is generated for each of the five simulated point targets, attention should be drawn to all Pareto efficient solutions for the points. The maximum steering angles and number of PWs corresponding to the

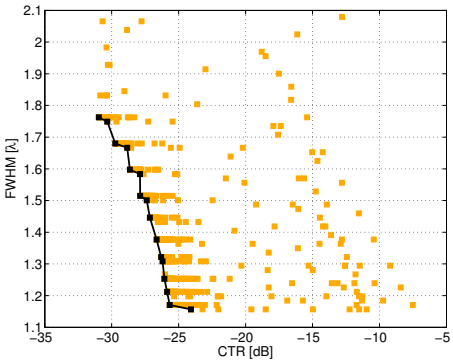

Fig. 2. Scatter plot of FWHM-CTR pairs from the simulated HR images at 9 mm for the λ-pitch transducer. Pareto optimal solutions are shown with black squares and the Pareto frontier as the black curve.

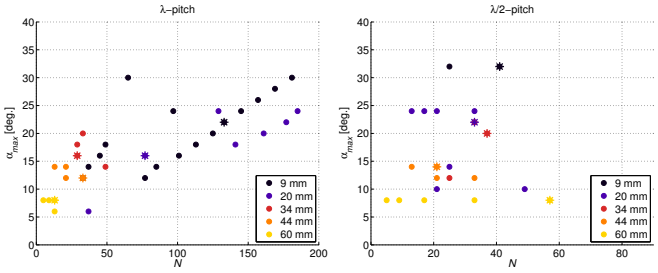

Fig. 3. Maximum steering angles α_{max} and number of emissions N corresponding to Pareto efficient solutions. Shown for each depth and for the λ-pitch (left) and λ/2-pitch transducer (right). Knee point solution from frontiers are marked with asterisks.

Pareto efficient solutions are shown in Fig. 3. The figures give an overview of the Pareto efficient solutions in addition to the knee point solutions from the frontier (marked with asterisks).

Deciding on a single combination of max steering angle and number of PWs for all depths is challenging. Here, a setup of 73 PWs and $\alpha_{max} = 22°$ is suggested for the λ-pitch transducer as a compromise between frame rate and a reduced image quality at 9 and 20 mm. It gives a FWHM $= 1.3\lambda$ and CTR $= -25$ dB at 9 mm. For the λ/2-pitch transducer, a setup of 37 PWs and $\alpha_{max} = 22°$ is chosen and gives FWHM $= 1.3\lambda$ and CTR $= -56$ dB. Furthermore, the simulations show that both transducers can obtain similar image quality with CTR < -40 dB for depths higher than 25 mm using the same setups, while the transducers have a difference in CTR of 15-25 dB down to 25 mm. This is investigated further in measurements.

III. EXPERIMENTAL METHODS

A B-mode imaging sequence was implemented on the experimental scanner SARUS [14] using the parameters listed in Table I. An interleaved sequence with emissions for a λ/2-pitch and λ-pitch transducer was used with a pulse repetition frequency of 5 kHz. A linear array transducer was employed, and with its 192 elements and 0.56λ pitch it has identical parameters to the λ/2-pitch transducer in Table I. By exciting the first and second element simultaneously, the third and fourth element simultaneously and so forth, a λ pitch trans-

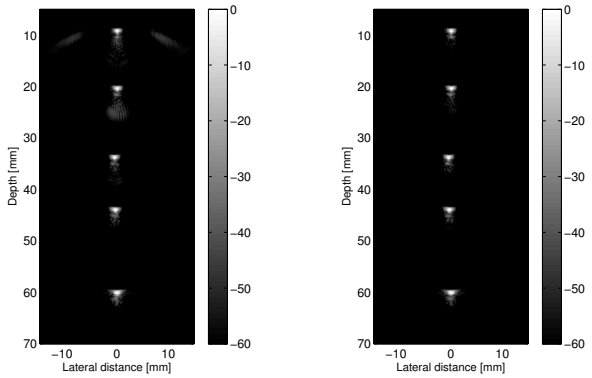

Fig. 4. B-mode image of wire phantom. Using the λ-pitch (left) and λ/2-pitch transducer (right), and 37 PWs with $\alpha_{max} = 22°$.

ducer with 96 elements is employed and emulating the λ-pitch transducer in Table I. Data were sampled and stored for all transducer elements and processed offline using the BFT3 toolbox [13]. For the λ-pitch transducer, data from element one and two, three and four, etc. were averaged. Two phantoms were scanned: a water tank phantom containing five wires, and a multi-tissue contrast phantom containing an anechoic cyst at 17 mm (Model 040GSE, CIRS Inc., Virginia, USA) with tissue attenuation of 0.5 dB/(cm·MHz).

IV. Experimental Results

A scan of the wire phantom is shown in Fig. 4 for the λ-pitch and λ/2-pitch transducer. The optimized setup for the λ/2-pitch transducer is used (N = 37 and α_{max} = 22°.). For the λ-pitch transducer, off-axis energy lobes and artefacts around the wires at 9 and 20 mm degrade the image quality compared to using the λ/2-pitch transducer.

The bottom image in Fig. 5 shows the PSF at 9 mm when using the optimized setup for the λ/2-pitch transducer, while the number of emissions have been varied for the λ-pitch transducer (three top images). CTR is quantified as a function of N for the PSF at 9 mm in Fig. 6, where α_{max} = 22°. While the measurements are in accordance with the simulations for the λ-pitch transducer, there is 15 dB difference for the λ/2-pitch transducer. The asymptotic trend of the measured CTR curve indicates that this is because a lower limit has been reached for the used imaging system. Note also, that the λ-pitch transducer never attains the same minimum CTR level as the λ/2-pitch transducer even for a high number of emissions.

In Fig. 7, measurements of the cyst phantom are shown. A similar degraded image quality as in Fig. 5 is observed for the λ-pitch transducer compared to the λ/2-pitch transducer as a function of N. The Contrast-to-Noise Ratio (CNR),

$$CNR = \frac{\mu_s - \mu_c}{\sqrt{\sigma_s^2 + \sigma_c^2}}, \tag{1}$$

was calculated for the cyst. μ_s and μ_c are the mean intensities of the cyst region and speckle region, while σ_s^2 and σ_c^2 are the corresponding variances. CNR is shown as a function of N in Fig. 7. Furthermore, using only 5 emissions as in blood

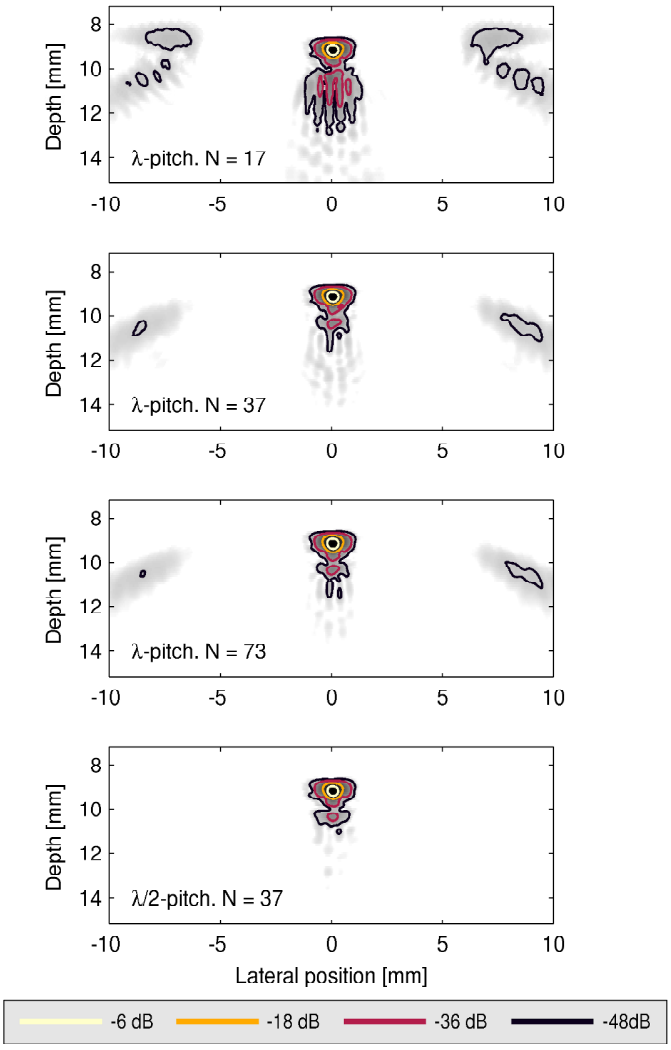

Fig. 5. Measured PSFs at 9 mm depth. The three top figures are for the λ-pitch transducer and the bottom figure is for the λ/2-pitch transducer. The maximum steering angle is 22°, and the number of emissions, N, is 17, 37, 73, and 37 for the four figures, respectively. The dynamic range is 60 dB.

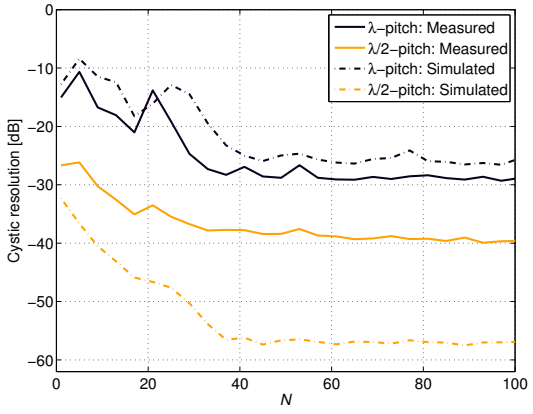

Fig. 6. Cystic resolution as a function of the number of emissions N for a α_{max} = 22°. For a PSF at 9 mm. Cystic resolution is shown for a λ and λ/2-pitch transducer and for simulated and measured data.

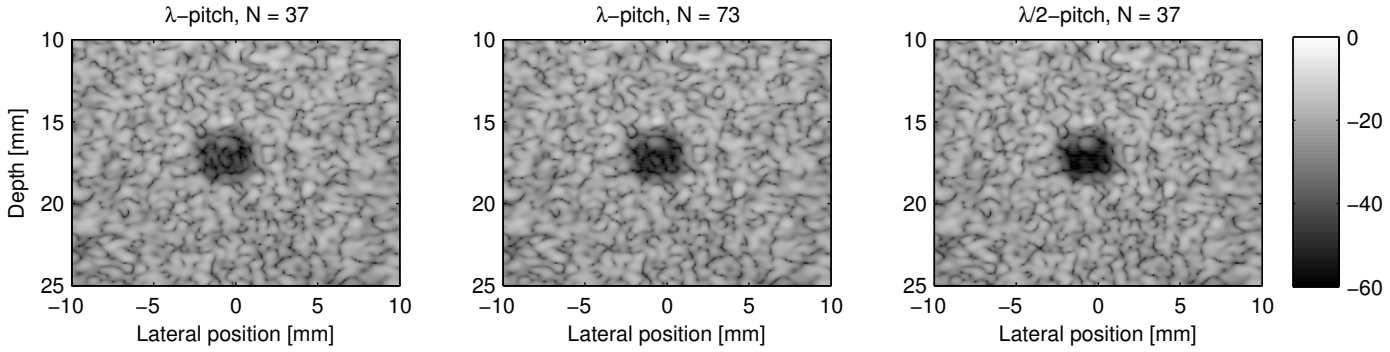

Fig. 7. PW imaging of an anechoic cyst embedded in a tissue mimicking phantom. The left and middle images are for the λ-pitch transducer and the right image is for the λ/2-pitch transducer. The number of emissions, N, is 17, 73, and 37 for the three figures, respectively. The maximum steering angle is 22°.

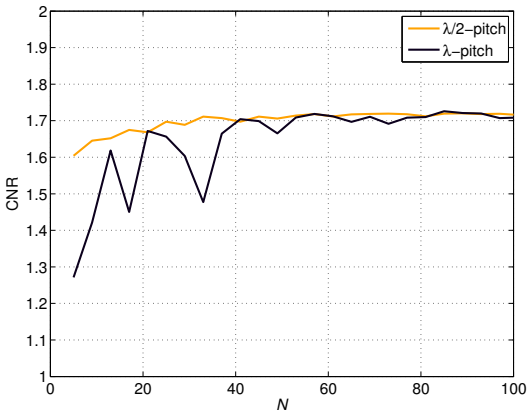

Fig. 8. The contrast-to-noise ratio (CNR) as a function of number of emissions N for the cyst at 17 mm. CNR is shown for the λ/2 and λ-pitch transducer.

flow estimation, peak intensities are -25 dB inside the cyst, which is undesirable and would give false flow velocities if the vessel wall is moving.

V. Conclusion

Image quality of PW images was investigated using a λ/2-pitch transducer and compared to a λ-pitch transducer. The number of PW emissions and steering angles were selected based on a proposed procedure for optimizing the image quality. For small parts imaging, it was demonstrated that the number of emissions could be decreased by almost half, from 73 to 37, by using a λ/2-pitch transducer rather than a λ-pitch transducer. The image quality was degraded to a depth of 25 mm due to grating lobes from a λ-pitch transducer, and it is therefore recommended always to use a λ/2-pitch transducer to avoid artefacts in SA/PW imaging and to increase the frame rate. Potentially, it can have an impact on the frame rate in anatomical imaging and flow estimation systems, and thus, increase the limit of maximum detectable velocities.

Acknowledgments

This work was supported by grant 82-2012-4 from the Danish National Advanced Technology Foundation and by BK Ultrasound.

References

[1] M. Karaman, P. C. Li, and M. O'Donnell, "Synthetic aperture imaging for small scale systems," *IEEE Trans. Ultrason., Ferroelec., Freq. Contr.*, vol. 42, pp. 429–442, 1995.

[2] J. A. Jensen, S. Nikolov, K. L. Gammelmark, and M. H. Pedersen, "Synthetic aperture ultrasound imaging," *Ultrasonics*, vol. 44, pp. e5–e15, 2006.

[3] M. Tanter, J. Bercoff, L. Sandrin, and M. Fink, "Ultrafast compound imaging for 2-D motion vector estimation: application to transient elastography," *IEEE Trans. Ultrason., Ferroelec., Freq. Contr.*, vol. 49, pp. 1363–1374, 2002.

[4] J. Y. Lu, "2D and 3D high frame rate imaging with limited diffraction beams," *IEEE Trans. Ultrason., Ferroelec., Freq. Contr.*, vol. 44, pp. 839–855, 1997.

[5] K. L. Gammelmark and J. A. Jensen, "Multielement synthetic transmit aperture imaging using temporal encoding," *IEEE Trans. Med. Imag.*, vol. 22, no. 4, pp. 552–563, 2003.

[6] G. Montaldo, M. Tanter, J. Bercoff, N. Benech, and M. Fink, "Coherent plane-wave compounding for very high frame rate ultrasonography and transient elastography," *IEEE Trans. Ultrason., Ferroelec., Freq. Contr.*, vol. 56, no. 3, pp. 489–506, March 2009.

[7] S. I. Nikolov and J. A. Jensen, "In-vivo Synthetic Aperture Flow Imaging in Medical Ultrasound," *IEEE Trans. Ultrason., Ferroelec., Freq. Contr.*, vol. 50, no. 7, pp. 848–856, 2003.

[8] J. Udesen, F. Gran, K. L. Hansen, J. A. Jensen, C. Thomsen, and M. B. Nielsen, "High frame-rate blood vector velocity imaging using plane waves: Simulations and preliminary experiments," *IEEE Trans. Ultrason., Ferroelec., Freq. Contr.*, vol. 55, no. 8, pp. 1729–1743, 2008.

[9] J. Bercoff, G. Montaldo, T. Loupas, D. Savery, F. Meziere, M. Fink, and M. Tanter, "Ultrafast compound Doppler imaging: Providing full blood flow characterization," *IEEE Trans. Ultrason., Ferroelec., Freq. Contr.*, vol. 58, no. 1, pp. 134–147, January 2011.

[10] K. Deb, "Multi-objective optimization," in *Search methodologies*. Springer, 2005.

[11] J. A. Jensen and N. B. Svendsen, "Calculation of pressure fields from arbitrarily shaped, apodized, and excited ultrasound transducers," *IEEE Trans. Ultrason., Ferroelec., Freq. Contr.*, vol. 39, pp. 262–267, 1992.

[12] J. A. Jensen, "Field: A program for simulating ultrasound systems," *Med. Biol. Eng. Comp.*, vol. 10th Nordic-Baltic Conference on Biomedical Imaging, Vol. 4, Supplement 1, Part 1, pp. 351–353, 1996.

[13] J. M. Hansen, M. C. Hemmsen, and J. A. Jensen, "An object-oriented multi-threaded software beamformation toolbox," in *Proc. SPIE Med. Imag.*, vol. 7968, March 2011, pp. 79 680Y 1–9.

[14] J. A. Jensen, H. Holten-Lund, R. T. Nilsson, M. Hansen, U. D. Larsen, R. P. Domsten, B. G. Tomov, M. B. Stuart, S. I. Nikolov, M. J. Pihl, Y. Du, J. H. Rasmussen, and M. F. Rasmussen, "SARUS: A synthetic aperture real-time ultrasound system," *IEEE Trans. Ultrason., Ferroelec., Freq. Contr.*, vol. 60, no. 9, pp. 1838–1852, 2013.